



JOHNS HOPKINS
BLOOMBERG
SCHOOL of PUBLIC HEALTH

Johns Hopkins University, Dept. of Biostatistics Working Papers

2-4-2011

POPULATION FUNCTIONAL DATA ANALYSIS OF GROUP ICA-BASED CONNECTIVITY MEASURES FROM fMRI

Shanshan Li

Johns Hopkins Bloomberg School of Public Health, Department of Biostatistics, shanshanli0627@gmail.com

Brian S. Caffo

Johns Hopkins Bloomberg School of Public Health, Department of Biostatistics

Suresh Joel

Kennedy Krieger Institute

Stewart Mostofsky

Kennedy Krieger Institute; Department of Neurology, Johns Hopkins School of Medicine

James Pekar

Kennedy Krieger Institute

See next page for additional authors

Suggested Citation

Li, Shanshan; Caffo, Brian S.; Joel, Suresh; Mostofsky, Stewart; Pekar, James; and Spear Bassett, Susan, "POPULATION FUNCTIONAL DATA ANALYSIS OF GROUP ICA-BASED CONNECTIVITY MEASURES FROM fMRI" (February 2011). *Johns Hopkins University, Dept. of Biostatistics Working Papers*. Working Paper 224. <http://biostats.bepress.com/jhubiostat/paper224>

This working paper is hosted by The Berkeley Electronic Press (bepress) and may not be commercially reproduced without the permission of the copyright holder.

Copyright © 2011 by the authors

Authors

Shanshan Li, Brian S. Caffo, Suresh Joel, Stewart Mostofsky, James Pekar, and Susan Spear Bassett

Population functional data analysis of group ICA-based connectivity measures from fMRI

Shanshan Li

Brian Caffo

Suresh Joel

Stewart Mostofsky

James Pekar

Susan Spear Bassett

Abstract

In this manuscript, we use a two-stage decomposition for the analysis of functional magnetic resonance imaging (fMRI). In the first stage, spatial independent component analysis is applied to the group fMRI data to obtain common brain networks (spatial maps) and subject-specific mixing matrices (time courses). In the second stage, functional principal component analysis is utilized to decompose the mixing matrices into population-level eigenvectors and subject-specific loadings. Inference is performed using permutation-based exact conditional logistic regression for matched pairs data. Simulation studies suggest the ability of the decomposition methods to recover population brain networks and the major direction of variation in the mixing matrices. The method is applied to a novel fMRI study of Alzheimer's disease risk under a verbal paired associates task. We found empirical evidence of alternative ICA-based metrics of connectivity in clinically asymptomatic at risk subjects when compared to controls.

1 Introduction

Functional MRI is a driving force in the field of brain mapping and cognitive neuroscience. Functional connectivity is the study of correlations in measured neural signals. Recently, attention in fMRI research has been focused on discovering spatial correlations in the BOLD (blood oxygen level dependent) signal, rather than functional activation related to a paradigm. Independent component analysis (ICA) and principal component analysis

(PCA) are popular exploratory data analysis techniques to account for unknown - yet structured - spatiotemporal processes in fMRI data (Beckmann and Smith 2004, 2005).

Spatial independent component analysis is an approach for decomposing fMRI data into spatial maps multiplied by their respective time courses, where the maps are drawn from spatial distributions that are statistically independent (Calhoun et al., 2001). The spatial independence assumption is well suited to the sparse nature of the spatial pattern for typical brain activation (McKeown and Sejnowski, 1998; Guo and Giuseppe, 2008). The time courses estimated from spatial ICA describe the temporal characteristics of functional networks, i.e. areas of temporal correlation in the BOLD signal. Variation in subjects' time courses reflects population heterogeneity in ICA-based metrics of connectivity.

We propose functional principal component analysis and regression (FPCA and FPCR) as unifying frameworks for analysis of temporal mixing matrices. FPCA is a common method to capture the main directions of variation and dimension reduction in a collection of functions (Ramsay and Silverman, 2005; Hall and Hosseini-Nasab, 2006; Di et al., 2008). We use FPCA to identify the population-level eigenvectors that characterize the geometric directions of variation of the time courses acquired from ICA. FPCA summarizes the subject-specific loadings, called principal component scores, by projecting subject curves on the basis of principal components (Di et al., 2008). PC scores can be used in functional regression, so called FPCR, to assess the effect of fMRI temporal patterns on diagnostic classification. Notably, we propose and implement a use of FPCA on temporal mixing matrices within the context of exact permutation-based conditional logistic regression to analyze risk status for Alzheimer's disease in matched-pairs study. That is, this manuscript considers investigating population variation in brain networks by summarizing temporal mixing matrices using functional PCA in conditional logistic regression.

The methodology is explored within the context of a longitudinal verbal paired associates paradigm fMRI study of subjects at high risk for Alzheimer's disease and controls. In this manuscript, we consider subjects with evidence for mild cognitive impairment at the time of scanning and closely matched asymptomatic controls. We note, however, that the methods are applicable without modification to resting state data as well.

The remainder of the paper is organized as follows. Section 2 describes the studied dataset. Section 3 introduces our two-stage method, which involves ICA on the group data in the first stage and PCA on the time courses of independent components in the second stage. Section 4 shows the performance of our procedure in an extensive simulation study. Section 5 provides the application of the two-stage methods to an ongoing study with 13 pairs of subjects, while Section 6 gives a discussion.

2 Data

The data derive from an ongoing study of Alzheimer's disease progression. This study follows roughly two hundred subjects, such that 100 were at high familial risk for AD while 100 were at low risk. Longitudinal imaging, biomarkers and a neuro-behavioral battery of tests were collected. Further details on the study can be found in Bassett et al. (2006).

Our analysis considers 26 subjects, of which 13 showed no evidence of cognitive decline and 13 were declared as mildly cognitive impaired. All 13 non-cases were from the low-risk group, while 11 of the 13 cases were from the high risk group. Control subjects were matched to cases via age, gender and education.

Three waves of neuroimaging data collection have been planned. Two have been completed. The fMRI data used in the analysis are from the second wave, which is concurrent with the measurements used to declare subjects as having MCI. All fMRI data used were part of a protocol that involved a verbal memory paradigm (see below).

Functional neuroimaging was obtained via a 1.5 T Philips Intera-NT scanner (Philips Medical Systems, Best, The Netherlands) at the F.M. Kirby Functional Imaging Research Center (Kennedy Krieger Institute, Baltimore, MD). The TR was 1,000 MS. Slices were acquired in a band focused on the medial temporal lobe. Hence, for example, much of the anterior portion of the component frontal and posterior portion of the occipital lobe were not studied.

The paradigm was an auditory word-pair association task. It consisted of two 6 min and 10 s sessions with each session having six sets of three blocks. Three types of blocks were considered: encoding, recall, and rest. When in the encoding block, subjects were presented with seven unrelated word pairs. When in the recall block, subjects were presented with the first word of each pair and instructed to silently recall the second. In the baseline block, subjects were presented with an asterisk.

3 Methods

3.1 Independent Component Analysis

Independent component analysis (ICA) is a commonly used method for recovering underlying independent sources from their mixtures, i.e. so-called blind source separation. ICA has been frequently utilized on the analysis of functional neuroimaging data since 1998 (McKeown et al., 1998a, 1998b; Calhoun et al., 2001; Guo and Giuseppe, 2008). Two key benefits of ICA are its empirical nature and its (often considered reasonable) underlying generative model. Specifically, it models collected signals as linear weighted

combinations of independent sources. Notationally, a noise-free ICA model specifies

$$X = AS,$$

where X is the data matrix (usually dimension reduced by an SVD), rows of S contain the non-Gaussian independent components and A is a linear mixing matrix. ICA attempts to obtain S by seeking an unmixing matrix W such that WX is a good approximation to the original sources S . Without further restrictions, this problem is not identified. Different implementations of ICA get around lack of identifiability by considering different criteria for estimation. FastICA is a fixed-point scheme frequently used for independent component estimation (see <http://www.cis.hut.fi/projects/ica/fastica/>) by iteratively maximizing negative entropy. It is easily accessible and subroutines have been made available for several scripting languages. We use fastICA as our optimization criteria in this manuscript, as it is a popular ICA fitting algorithm, though note that the proposed modeling strategy is largely agnostic to this choice. Note further that we use a so-called ‘noise-free’ ICA model. Of course, such assumptions are not realistic for fMRI and hence measurement error and other sources of variation will be absorbed in the estimated time courses and spatial maps. Our simulations, however, show that this does not impact our regression approach. Regardless, we reiterate that one could use a probabilistic ICA method (Beckmann and Smith, 2004) for estimation instead.

There are a wide variety of group ICA approaches for multi-subject fMRI data (see Calhoun et al., 2009), in this paper we use temporal concatenation approach, also called spatial group ICA, as introduced by Calhoun et al. (2001). Figure 1 illustrates the details of spatial group ICA. Each subject’s data can be decomposed into the outer products of spatially independent components and associated time courses. However, we do not decompose the data individually, because independent components are not ordered (as in the case of principal component analysis), and it is difficult to identify matching components across subjects. Instead, by assuming common spatial maps, we can concatenate all subjects’ data in the temporal domain, and apply ICA to the aggregated data matrix. The group mixing matrix is the concatenated time course for all subjects (Figure 1 B). Individual mixing matrices can be backreconstructed by partitioning the group mixing matrix into submatrices corresponding to each subject (Figure 1 A). Inferences will be made on those individual mixing matrices.

Following the notations in Guo and Giuseppe (2008), let $i = 1, \dots, N$ index subjects, $t = 1, \dots, T$ index time points, and $v = 1, \dots, V$ index voxels. Let X_i be a $T \times V$ data matrix for subject i . The group ICA model can be expressed as

$$X = MS, \tag{1}$$

where $X = [X_1^t, \dots, X_N^t]^t$ is the $NT \times V$ group data matrix formed by concatenating N subjects' data in the temporal domain. Assume there are q independent components, then S is a $q \times V$ matrix containing q statistically independent spatial maps in its rows. $M = [A_1^t, \dots, A_N^t]^t$ is the $NT \times q$ group mixing matrix, where A_i is the $T \times q$ submatrix corresponding to the i th subject. Let $A^{(k)} = [A_1^{(k)}, A_2^{(k)}, \dots, A_N^{(k)}]$, where $A_i^{(k)}$ is the k th column of A_i , $k = 1, 2, \dots, q$. $A_i^{(k)}$ is the time course associated with the k th spatial map for subject i . $A^{(k)}$ can be acquired by reshaping the k th column of M to a $T \times N$ matrix.

3.2 Principal Component Analysis and Generalized Functional Regression

Generalized functional regression is a powerful tool to explore the association between functional variables and scalar outcomes, such as binary disease outcomes (Ramsay and Silverman, 2006; Crainiceanu et al., 2009a; Goldsmith et al., 2010). Here, we propose the functional variables to be the individual mixing matrices, which ideally characterize the temporal patterns in brain networks. We start with univariate functional analysis. That is, by fixing k a specific index for the independent component, we only consider one functional regressor at a time, though acknowledge that multivariable regression models are a relatively straightforward extension. Assume for each subject i , Y_i is the scalar outcome, $A_i^{(k)}$ are random functions, and Z_i is a vector of nonfunctional covariates. Without loss of generality, we assume $A_i^{(k)}$ are mean zero stochastic processes (which can be achieved by subtracting the population average function). A generalized linear functional model can be expressed as (Crainiceanu et al., 2009a):

$$\begin{cases} Y_i \sim EF(\mu_i, \eta); \\ g(\mu_i) = \alpha + \int_0^T A_i^{(k)}(s)\beta^{(k)}(s)ds + Z_i^t\gamma. \end{cases} \quad (2)$$

Here $EF(\mu_i, \eta)$ denotes an exponential family distribution with mean μ_i and dispersion parameter η . The functional parameter $\beta(\cdot)$ is the main target of inference. The functional component of model (2) is basically a weighting scheme, which tends to emphasize or de-emphasize components of the regressor. In our context, it relates the temporal mixing matrices to the disease status outcomes.

We use Functional Principal Component Analysis (FPCA) to estimate the first few eigenvectors that capture most of the variability of the space spanned by $A_i^{(k)}$ across subjects. This simultaneously yields a convenient, data-driven basis for which to decompose model (2) into easily estimated parts, as well as recasts the problem in the terms of the greatest direction of inter-subject variation in the temporal mixing of ICA-based brain networks. To simplify notation, we omit the index k in the following illustration.

FPCA considers a complex functional regression space by decomposing the covariance operator $K_A(t, s) = \text{Var}\{A_i(t), A_i(s)\}$. The spectral decomposition of the covariance matrix is given by $K_A(t, s) = \sum_{j=1}^{\infty} \lambda_j \psi_j(t) \psi_j(s)$ (as noted in Di et al., 2008, via Mercer's theorem, Indritz 1963 chapter 4), where $\lambda_1 \geq \lambda_2 \geq \dots$ are the ordered eigenvalues and $\psi_j(\cdot)$ are the associated orthonormal eigenfunctions. The spectral decomposition yields a parsimonious expansion of the subject level functions $A_i(t) = \sum_{j=1}^{\infty} \xi_{ij} \psi_j(t)$, referred to as the *Karhunen/Loève* (KL) decomposition (Karhunen, 1947; Loève, 1945). Here, $\xi_{ij} = \int_0^T A_i(t) \psi_j(t) dt$ are referred to as the principal component scores. Distributionally, $E(\xi_{ij}) = 0$, $\text{Var}(\xi_{ij}) = \lambda_j$ and $\text{Cov}(\xi_{ij}, \xi_{i'j'}) = 0$ for every i and $j \neq j'$. For practicality, we truncate the decomposition at L terms (though see Goldsmith et al., 2010). We follow the approach proposed by Di et al. (2008) to estimate L based on proportion of variance explained. Let P_1 and P_2 be two thresholds, and define

$$L = \min\{k : \sum_{j=1}^k \lambda_j / \sum_{j=1}^{\infty} \lambda_j \geq P_1, \lambda_k < P_2\}.$$

Here, P_1 stands for the cumulative explained variance threshold and P_2 stands for the individual explained variance. In this manuscript, we choose $P_1 = 0.95$ and $P_2 = 0.02$. These choices work well in our simulations and application. However, they should be carefully tuned in other settings, perhaps using simulations.

The true mixing matrices are not observed. Instead we obtain the model-based estimates from the fastICA algorithm (Crainiceanu et al., 2009b). (Note, of course, the fact that the ICA algorithm we are using does not assume noise does not mean that there is actually no noise in the estimated time courses.) Hence, assume we get noisy signals $W_i(t) = A_i(t) + \epsilon_i(t)$, where $\epsilon_i(t)$ is a white noise process with variance σ_{ϵ}^2 . Under this assumed model, the covariance operator for the observed data is $K^W(s, t) = K^A(s, t) + \sigma_{\epsilon}^2 \delta_{ts}$, where $K^W(s, t) = \text{Cov}\{W_i(s), W_i(t)\}$, $K^A(s, t) = \text{Cov}\{A_i(s), A_i(t)\}$, and $\delta_{ts} = 1$ if $t = s$ and is 0 otherwise (Di et al., 2008). This equation reveals that the diagonal elements of $K^W(s, t)$ incorporate the nugget measurement error. A simple and natural solution is to drop the diagonal elements and smooth the covariance matrix. We use the standard (moment based) estimate $\hat{K}^W(s, t)$ of $K^W(s, t)$ from the observed data. Second, estimate $\hat{K}^A(s, t)$ by smoothing $\hat{K}^W(s, t)$ for $s \neq t$, as suggested by Staniswalis and Lee (1998) and Yao et al. (2003). The eigenvalues λ_j and eigenfunctions $\xi_j(\cdot)$ can then be derived from $\hat{K}^A(s, t)$ (Di et al., 2008).

Once the eigenfunctions, $\psi_j(\cdot)$, and truncation lag, L , are fixed, the model for the

noisy signals can be written as:

$$\begin{cases} W_i(t) = \sum_{j=1}^L \xi_{ij} \psi_j(t) + \epsilon_i(t); \\ \xi_{ij} \sim N(0, \lambda_j); \epsilon_i(t) \sim N(0, \sigma_\epsilon^2). \end{cases} \quad (3)$$

As stated in Crainiceanu et al. (2009a), this is a linear mixed model with random effects ξ_{ij} used in the outcome model.

Since $\{\psi_j(t)\}$ is an orthonormal basis in $L_2[0, T]$, both $A_i(t)$ and $\beta(t)$ have unique representations $A_i(t) = \sum_{j \geq 1} \xi_{ij} \psi_j(t)$, $\beta(t) = \sum_{j \geq 1} \beta_j \psi_j(t)$ and equation (2) can be rewritten as:

$$\begin{cases} Y_i \sim EF(\mu_i, \eta); \\ g(\mu_i) = \alpha + \sum_{j=1}^L \xi_{ij} \beta_j + Z_i^t \gamma. \end{cases} \quad (4)$$

Following the definition of Crainiceanu et al. (2009a), model (3) is the exposure model and model (4) is the outcome model. In our context, the exposure model considers the temporal mixing matrices from group ICA; the outcome model relates the principal components from the exposure model to a disease status outcome model. As disease status is fixed (the 13 control subjects were matched to the 13 cases), the outcome model employs logits hence using traditional case-control logistic regression (Prentice and Pyke, 1979; Breslow and Cain, 1988). We first estimate the random effects ξ_{ij} in model (3) using FPCA, and plug them in model (4).

Since there are q components of the mixing matrix M , we can extend the model to the case of multiple functional regressors.

$$\begin{cases} Y_i \sim EF(\mu_i, \eta); \\ g(\mu_i) = \alpha + \int_0^T A_i^{(1)}(s) \beta^{(1)}(s) ds + \dots + \int_0^T A_i^{(q)}(s) \beta^{(q)}(s) ds + Z_i^t \gamma. \end{cases} \quad (5)$$

Similarly, equation (5) can be rewritten as

$$g(\mu_i) = \alpha + \sum_{j=1}^{L_1} \xi_{ij}^{(1)} \beta_j^{(1)} + \dots + \sum_{j=1}^{L_q} \xi_{ij}^{(q)} \beta_j^{(q)} + Z_i^t \gamma.$$

This extension is, in principle, trivial to implement once the PC scores are obtained. However, with small numbers of subjects, large multivariate models are not realistic options. Hence, in our study we investigate variables one or two at a time.

Another extension is to study the association between functional connectivity (Friston et al., 1993, 1994) and diagnostic classification. Functional connectivity is biologically

meaningful because it is assumed that “memory and other cognitive abilities are the result of the integrated activity in networks of regions, rather than activity in any one region in isolation” (Grady et al., 2001). Joel et al. (in press) argue for the important interpretation of inter- and intra-network connectivity ostensibly measured by the correlation and variance of the temporal mixing matrices respectively. As these matrices have zero mean, we consider their products and squares. Mathematically, ICA-based inter-network functional connectivity is defined as (Joel et al., in press):

$$\int A^{(k)}(t)A^{(k')}(t)dt,$$

and intra-network functional connectivity is defined as

$$\int A^{(k)}(t)^2dt,$$

where $A^{(k)}(t)$ is the time course modulating spatial map k , and $A^{(k')}(t)$ is the time course modulating spatial map k' .

To study the association between inter-network functional connectivity and the outcomes, i.e. Alzheimer’s disease, we apply functional regression on the product of time courses associated with two different spatial maps:

$$\begin{cases} Y_i \sim EF(\mu_i, \eta); \\ g(\mu_i) = \alpha + \int_0^T A_i^{(k)}(s)A_i^{(k')}(s)\beta(s)ds + Z_i^t\gamma. \end{cases} \quad (6)$$

Notice that if $\beta(s)$ is estimated to be a constant, then model (6) simply regresses the outcome on the measure of inter-network connectivity suggested by Joel et al. (in press). Similarly, to study the association between intra-network functional connectivity and the health outcomes, we apply functional regression on the squares of time courses associated with one spatial map:

$$\begin{cases} Y_i \sim EF(\mu_i, \eta); \\ g(\mu_i) = \alpha + \int_0^T A_i^{(k)}(s)^2\beta(s)ds + Z_i^t\gamma. \end{cases} \quad (7)$$

Again, notice if $\beta(s)$ is a constant, this model corresponds to regressing the outcome on the measure of intra-network connectivity suggested by Joel et al. (in press).

3.3 Related Work

Beckmann and Smith (2005) proposed a tensor PICA model, which factors the group data as a trilinear combination of three outer products, representing group spatial maps and time courses but subject-specific loadings. The tensor PICA is a simplified version

of our model in the sense that, by assuming common time courses, they only retain one eigenvector in the PCA stage. We can check the validity of their model by calculating the ratio of the largest eigenvalue and the sum of all the eigenvalues. Their approach may not work well if the temporal dynamics are different across subjects, such as in a resting state study (Calhoun et al., 2009). Our method allows heterogeneity in time courses and hence is more robust.

An alternative two-stage decomposition for the analysis of fMRI data was proposed by Caffo et al. (2010). Their approach first used singular value decomposition (SVD) to obtain subject-specific eigenimages (spatial maps) and eigenvariates (time series). Then the collections of eigenimages and eigenvariates were decomposed to form population-level brain networks and time series. Subject-level data were projected onto these population eigenvectors to obtain subject-specific loadings and those loadings can be used in generalized functional regression. One potential weakness of their approach is the ignorance of variance ordering of subject-specific eigenvectors in the population analysis. Comparatively, the components in ICA are not ordered, so the problem is avoided. In addition, the SVD forces orthogonal eigenimages and eigenvariates, which may or may not reflect actual biology. In principle, the relevant information content of ICA-based regressors is equivalent to SVD-based regressors for FPCA. However, the ICA-based regressors tend to be more interpretable by not requiring orthogonality of the time courses. In addition, our use of group ICA adds a level of parsimony, by assuming common brain networks across subjects (see Calhoun et al., 2001). In contrast, the methods of Caffo et al. (2010) consider separate spatial networks for each subject.

4 Simulation

We conducted a simulation study to investigate the properties of two-stage decompositions for group fMRI data. In our simulation, assume there are $I = 50$ subjects, $q = 3$ independent components. Each spatial map contains $V = 64 \times 64$ elements, while each time course contains $T = 80$ time points. For time courses associated with each independent component, assume there are $n = 2$ eigenvalues and eigenfunctions. The estimation parameters are listed in table 1. The underlying spatial maps and the eigenfunctions for time courses are depicted in Figure 2. We consider a variety of scenarios, according to different amount of noise. The signals are standardized and the deviation for the noise is 0 (no noise), 0.3 (moderate), 1 (large) respectively. We conducted 100 simulations for each scenario.

Figure 3 displays the accuracy of the simulation results. The spatial correlation is the absolute correlation between the estimated spatial map and the true spatial map without

noise. In the case of no noise, the mean of the spatial correlation is 0.998 ($SD < 0.001$) across the three independent components. For moderate noise, the mean of the spatial correlation is 0.946 ($SD < 0.001$) across the three independent components. For large noise, the mean of the spatial correlation is 0.946 ($SD < 0.001$). The results reveal that the quality of the recovered image is not affected by the amount of noise, within the range of signal to noise considered. The variation of the estimation results is very small, which indicates a level of robustness in the estimation method.

The temporal correlation is the absolute correlation between the estimated principal components of the time courses and the true principal components of the time courses. For the noise-free scenario, the mean of the absolute correlation for the first eigenfunction (PC 1) is 0.973 ($SD = 0.021$) across the three independent components; the mean of the absolute correlation for the second eigenfunction (PC 2) is 0.973 ($SD = 0.021$) across the three independent components. For moderate noise, the mean of the absolute correlation for the first eigenfunction (PC 1) is 0.975 ($SD = 0.023$) across the three independent components; the mean of the absolute correlation for the second eigenfunction (PC 2) is 0.975 ($SD = 0.023$) across the three independent components. For large noise, the mean of the absolute correlation for the first eigenfunction (PC 1) is 0.974 ($SD = 0.024$) across the three independent components; the mean of the absolute correlation for the second eigenfunction (PC 2) is 0.973 ($SD = 0.023$) across the three independent components. The results indicate that the principal components for time courses are also estimated very well. The bias is negligible, even in the case of large noise.

5 Application

We apply our method to a novel fMRI study of Alzheimer's disease risk under a verbal paired associates task. The study population, scanning methods and description of the paradigm are described in section 2 (also see Caffo et al., 2010). This study is part of an ongoing longitudinal study of Alzheimer's disease risk. In this particular analysis, we focus on 26 subjects, 13 of which meet criteria for mild cognitive impairment (MCI) with 13 matched controls. The fMRI data contains $79 \times 95 \times 68 = 510340$ voxels measured at 370 time points, with a TR of 1000 MS, for each subject. A group data matrix is generated by concatenating 26 subjects' fMRI data in the temporal domain. The aggregated matrix has dimension $NT \times V$, where $N = 26$, $T = 370$ and $V = 510340$.

In the practical application of ICA, identifying the number of independent components is an important step. For fMRI, the number of informative components is often assumed to be less than the spatial or temporal dimension; further the mathematics mandate that the number of ICs be less than the smaller of NT and V (typically NT). This manuscript

adopts a simple approach to estimate the number of components based on the eigenvalues of the covariance matrix.

It is easy to show that based on model (1), the covariance matrix of X can be expressed as:

$$C_x = \sum_{i=1}^q M_i M_i^T + \sigma^2 I,$$

where M_i is the i th column of M , q is the number of independent component, I is the identity matrix with dimension $NT \times NT$ (Hyvärinen et al. 2001). The eigenvalues are now the eigenvalues of $\sum_{i=1}^q M_i M_i^T$ plus a constant σ^2 . But the matrix $\sum_{i=1}^q M_i M_i^T$ has at most q nonzero eigenvalues, so the first q eigenvalues of C_x form a decreasing sequence with the rest eigenvalues being constant σ^2 :

$$d_1 > d_2 > \dots > d_q > d_{q+1} = d_{q+2} = \dots = d_{NT} = \sigma^2.$$

Figure 4 (the scree plot) shows the first 80 ordered eigenvalues of the group matrix. By visual inspection, the eigenvalues decay to a constant roughly at 30. So we apply ICA on the group data matrix specifying there are 30 independent components. The retention of all 30 components in subsequent modeling could potentially have issues of variance inflation. Moreover, we stipulate that the choice is admittedly ad hoc. We do not address this further in this manuscript, though emphasize the importance of performing sensitivity analysis to the number of retained eigenvalues. In addition, we do note success in using penalties terms in functional regression (see Goldsmith et al., 2010) that are insensitive to the choice of the number of components.

In the second stage, PCA is performed on the time courses for each independent component acquired from ICA. We then apply functional logistic regression on the scores derived from PCA, accounting for case-control matching. We first consider univariate regression analysis, that is, we conduct 30 regressions, with each regression on time courses associated with one specific spatial map. In our context, model (2) becomes

$$\text{logit}\{P(D_{ip} = 1|\alpha_p)\} = \alpha_p + \int_0^T A_i^{(k)}(s)\beta^{(k)}(s)ds, \quad (8)$$

where $k \in \{1, 2, \dots, 30\}$ is the index for independent component, $p \in \{1, 2, \dots, 13\}$ is the index for pair, α_p is the pair-specific random effect, $D_{ip} \in \{0, 1\}$ represents the risk status for subject i in pair p . Let $\{\psi_j^{(k)}(\cdot)\}$ be the eigenfunctions for $\{A_i^{(k)}(\cdot)\}$, then $\beta^{(k)}(s)$ can be written as $\beta^{(k)}(s) = \sum_{j=1}^L \beta_j^{(k)} \psi_j^{(k)}(s)$. Thus, model (8) becomes

$$\text{logit}\{P(D_{ip} = 1|\alpha_p)\} = \alpha_p + \sum_{j=1}^L \xi_{ij}^{(k)} \beta_j^{(k)},$$

which is a conditional logistic regression model with subject level PC scores as predictors. Since we only have 26 subjects in our dataset, the sample size is not large enough for

asymptotic results to be valid. We conduct permutation test to calculate the SE of the predictors. The idea is to permute all the possible outcomes, get the likelihood ratio test (LRT) statistic under each scenario, and calculate the probability that the LRT statistic from a random set of outcomes exceeds the actual observed LRT statistic. The null permutation distribution in this case (matched binary pairs) is equivalent to randomly permuting case status among matched pairs. Thus, each matched pair will have exactly one case and one control in every permutation. This permutation test is a special case of conditional logistic regression (Agresti, 2002). Our statistical inferences are based on the p-value calculated from the permutation distribution. No adjustment for multiplicity is made as our results are exploratory in nature.

Table 2 summarizes the regression results. Figure 5 exhibits the eigenfunctions of time courses that are associated with significant PC scores. Some predictors are negatively associated with odds of Alzheimer's disease, including the first PC score of time courses modulating spatial map 13, the third PC score of time courses modulating spatial map 19 and the first PC score of time courses modulating spatial map 26. For example, a subject with one unit higher in the first PC of time courses modulating spatial map 13 has $e^{-5.44} = 0.004$ times the odds of AD. After standardization, one standard deviation increase in the first PC score of time courses modulating spatial map 13 is associated with an odds ratio $e^{-1.60} = 0.202$. Other predictors are positively associated with Alzheimer's disease, including the second PC score of time courses modulating spatial map 11, the fourth PC score of time courses modulating spatial map 22 and the first PC score of time courses modulating spatial map 28. After standardization, one standard deviation increase in the first PC score of time courses modulating spatial map 28 is associated with an odds ratio $e^{1.60} = 4.95$.

Univariate analysis reveals that spatial maps 11, 13, 19, 22, 26, 28 are regions of interest, that is, their corresponding PC scores are significant predictors in models (3) and (4). Figure 6 exhibits three-D rendering of these spatial maps. Figure 7 displays brain regions that have over 20% overlap with the identified spatial maps, based on the anatomical parcellation given in Tzourio-Mazoyer et al., (2002). IC number 11 loads primarily on the temporal lobe and a small portion of the cerebellum in the imaging area. IC 19 covers the majority of cerebellum and vermis areas. IC 28 also covers the cerebellum and vermis areas. IC 22 loads specifically on the Heschl gyrus and the superior portion of the temporal lobe. IC 26 loads heavily on the cerebellum and the Heschl gyrus. Note that the spatial maps and time courses of ICA are unique only up to scalings, thus the positive and negative regions could be reversed without loss of information (Caffo et al., 2010).

A clinically interesting question is whether network interaction is related to diagnostic

classification. To study the association between inter-network functional connectivity and the adverse health outcomes, i.e. Alzheimer’s disease, we apply conditional logistic regression on the product of time courses associated with two different spatial maps. In our context, after accounting for pair matching, model (6) becomes

$$\text{logit}\{P(D_{ip} = 1|\alpha_p)\} = \alpha_p + \int_0^T A_i^{(k)}(s)A_i^{(k')}(s)\beta(s)ds,$$

where $k, k' \in \{11, 13, 19, 22, 26, 28\}$ and $k \neq k'$. If taking the product of $A_i^{(k)}(s)$ and $A_i^{(k')}(s)$ as a new function, all the procedures in univariate regression will follow immediately. Similarly, to study the association between intra-network connectivity and the adverse health outcomes, model (7) becomes

$$\text{logit}\{P(D_{ip} = 1|\alpha_p)\} = \alpha_p + \int_0^T A_i^{(k)}(s)^2\beta(s)ds.$$

The results are listed in table 3. After standardization, one standard deviation increase in the second PC score of the integrated activity of network 19 and 28 is associated with an odds ratio $e^{-1.6} = 0.214$; one standard deviation increase in the second PC score of the integrated activity of network 22 and 28 is associated with an odds ratio $e^{-1.30} = 0.273$; one standard deviation increase in the third PC score of the integrated activity within network 26 is associated with an odds ratio $e^{-1.74} = 0.176$.

6 Discussion

In this manuscript, we use temporal concatenation of multi-subjects’ data for group ICA. There are other competing group ICA approaches in the literature. Calhoun et al. (2009) reviewed that the existing group ICA approaches can be separated into five categories: temporal concatenation, spatial concatenation, pre-averaging, combining single subject ICA, and tensor-based approaches. Schmithorst and Holland (2004) compared the first three group ICA methods and concluded that temporal concatenation appears to work better for fMRI data. Therefore, we employ temporal concatenation, which allows for unique time courses for each subject, but assumes common group maps. From a biological perspective, this is akin to assuming that there are common group-level spatial brain networks, but how those networks mix over time varies by subject. Indeed, spatial group ICA has so far dominated the application of group ICA to fMRI. Practically, it is computational easier to have the ICs be the larger index. Biologically, the assumption that the maps are drawn from distributions which are statistically independent is consistent with the principle of segregation of brain function, or the idea that ‘different parts of the brain do different things’.

Figure 7 displays the overlap of the spatial maps and a parcellation of the template brain (Tzourio-Mazoyer et al., 2002). Because of the narrow imaging area, the spatial independent components overlap heavily on temporal regions. The most significant predictor is IC number 22. This map is primarily located in the temporal poles, olfactory areas and Heschl regions. This mirrors results found in (Caffo et al., 2010) who noted that these regions are areas of known interest in AD. In addition, a less significant region, 13, overlaps with the hippocampus, the primary brain region of interest in the study of AD. Note specifically that most of these spatial maps intersect with the olfactory areas, which have been hypothesized to be associated with neurodegenerative disorders and Alzheimer's disease in particular (see Mesholam et al., 1998). Looking across regions, the temporal poles, Heschl regions, cerebellum, amygdala and limbic olfactory areas are widely implicated across ICs. However, the results are non-specific.

These results must be viewed with caution given the large number of tests performed and the small number of MCI cases available for study. Moreover, the analysis was largely exploratory, without a priori regional hypotheses.

One difficulty of analyzing fMRI data is its high dimensionality. Existing algorithms may break down or become less reliable when performing on very large data sets. Our approach includes two steps. In the first stage, we attempt to decompose a group matrix with dimension $NT \times V$. In the second stage, we perform PCA on the time courses matrix with dimension $N \times T$. Hence, the computational time is mostly spent on the first stage group ICA. For studies with large number of subjects, the $NT \times V$ matrix may be too large in both dimensions to admit group ICA without dimensionality reduction. By conducting data reduction in the temporal domain, we could reduce one dimension of the large matrix to make it computationally practicable (Calhoun et al., 2001; Beckmann and Smith, 2005). More precisely, we perform PCA on the aggregated data set obtained by using temporal concatenation of all subjects' data, i.e. $Y_{T \times NV} = [X_1, \dots, X_N]$. Each subject's data is then projected onto the common subspace spanned by the first R eigenvectors, thus reduced to a $R \times V$ matrix. Accordingly, the group data matrix would be reduced to a $NR \times V$ matrix. In this manuscript, $N = 26$, so it is computationally manageable without subject-specific dimension reduction in the temporal domain. For studies with large number of participants, such data dimension reduction is a necessary preprocessing step. ICA on the reduced data will yield a mixing matrix with dimension $NR \times q$, where q is the number of independent components. The mixing matrix can be transformed back to the original scale $NT \times q$, as illustrated in Beckmann and Smith (2005); Guo and Giuseppe (2008).

This manuscript addresses decomposition methods to evaluate cross-sectional variation in brain networks. However, it can be easily extended to hierarchical models.

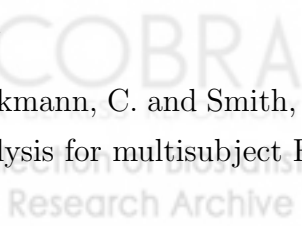
Longitudinal functional imaging studies are becoming increasingly common. For example, subjects may have fMRI records at multiple visits. Our two-stage method can be generalized for multi-level data very easily. In the first stage, we concatenate individual subjects' data in the temporal domain across all visits. That is, given J visits per subject, $Y_{NTJ \times V} = [X_{11}^t, \dots, X_{1J}^t, X_{21}^t, \dots, X_{2J}^t, \dots, X_{N1}^t, \dots, X_{NJ}^t]^t$ is the concatenated data matrix, where X_{ij} is the $T \times V$ matrix representing fMRI data for subject i at visit j . Decomposition of Y by spatial ICA yields a compound mixing matrix of dimension $NTJ \times q$, where q is the number of independent components. Subject and visit specific time courses can be acquired by partitioning the group mixing matrix. In the second stage, multilevel functional principal component analysis (Di et al. 2008) can be applied on the time courses to identify and quantify the subject-specific and subject/visit specific variation. Subject-specific loadings on principal components can be utilized as predictors to quantify the association between neuro-imaging signals to diagnostic classification. If we are interested in changes of time courses over visits, longitudinal functional principal component analysis (Greven et al., 2010) can be utilized as an extension of MFPCA. MFPCA only allows for random intercept, whereas LFPCA allows for both random intercept and random slope of time, thus is a more generalized model to deal with multi-level functional data.

Acknowledgements

The authors are grateful for support provided by NIH grant RO1 AG 016324.

References

- [1] Agresti, A. (2002). *Categorical Data Analysis (Wiley)*
- [2] Bassett, S., Yousem, D., Cristinzio, C., Kusevic, I., Yassa, M., Caffo, B., and Zeger, S. (2006). Familial risk for Alzheimers disease alters fMRI activation patterns. *Brain*, 129(5):1229.
- [3] Beckmann, C. and Smith, S. (2004). Probabilistic independent component analysis for functional magnetic resonance imaging. *IEEE Trans. Med. Imaging*, 23 (2), 137-152.
- [4] Beckmann, C. and Smith, S. (2005). Tensorial extensions of independent component analysis for multisubject FMRI analysis. *Neuroimage*, 25, 294-311.



- [5] Breslow, N. and Cain, K. (1988). Logistic regression for two-stage case-control data. *Biometrika*, 75 (1), 11-20.
- [6] Caffo, B., Crainiceanu, C., Verduzco, G., Mostofsky, S., Bassett, S., and Pekar, J. (2010). Two-stage decompositions for the analysis of functional connectivity for fMRI with application to Alzheimer's disease risk. *Neuroimage*, 51, 1140-1149.
- [7] Calhoun, V., Adali, T., Pearlson, G., and Pekar, J. (2001). A method for making group inferences from functional MRI data using independent component analysis. *Hum. Brain Mapp*, 14, 140-151.
- [8] Calhoun, V. , Liu, J., and Adall, T. (2009). A review of group ICA for fMRI data and ICA for joint inference of imaging, genetic, and ERP data. *Neuroimage*, 45, S163-S172.
- [9] Crainiceanu, C., Staicu, A., and Di, C. (2009a). Generalized Multilevel Functional Regression. *Journal of the American Statistical Association*, 104, 1550-1561.
- [10] Crainiceanu, C., Caffo, B., Di, C., and Punjabi, N. (2009b). Nonparametric signal extraction and measurement error in the analysis of electroencephalographic activity during sleep. *Journal of the American Statistical Association*, 104(486), 541-555.
- [11] Di, C., Crainiceanu, C., Caffo, B., and Naresh, P. (2008). Multilevel functional principal component analysis. *Annals of Applied Statistics*, 3(1), 458-488.
- [12] Goldsmith, J., Feder, J., Crainiceanu, C., Caffo, B., and Reich, D. (2010). Penalized Functional Regression. *Journal of Computational and Graphical Statistics*.
- [13] Friston, K., Frith, C., Liddle, P., and Frackowiak, R. (1993). Functional connectivity: The principal component analysis of large (PET) data sets. *J Cereb Blood Flow Metab*, 13, 5-14.
- [14] Friston, K. (1994). Functional and effective connectivity in neuroimaging: a synthesis. *Human Brain Mapping*, 2.
- [15] Grady, C., Furey, M., Pietrini, P., Horwitz, B., and Rapoport, S. (2001). Altered brain functional connectivity and impaired short-term memory in Alzheimers disease. *Brain*, 124(4), 739.
- [16] Greven, S., Crainiceanu, C., Caffo, B., and Reich, D. (2010). Longitudinal Functional Principal Component Analysis. *Electronic Journal of Statistics*, 4, 1022-1054.

- [17] Guo, Y. and Giuseppe, P. (2008). A unified framework for group independent component analysis for multi-subject fMRI data. *NeuroImage*, 42, 1078-1093.
- [18] Hall, P. and Hosseini-Nasab, M. (2006). On properties of functional principal components analysis. *Journal of the Royal Statistical Society Series B (Statistical Methodology)*, 68(1), 109-126.
- [19] Hyvärinen, A. Karhunen, J., and Oja, E. (2001). Independent Component Analysis *John Wiley and Sons*.
- [20] Hyvärinen, A. and Oja, E. (2000). Independent Component Analysis: Algorithms and Applications, *Neural Networks*, 13, 411-430.
- [21] Indritz, J. (1963). Methods in analysis. *Macmillan and Colier-Macmillan*.
- [22] Joel, S., Caffo, B., van Zijl, P., and Pekar, J. (in press). On the relationship between seed-based and ICA-based measures of functional connectivity *Magn. Reson. Med*.
- [23] Karhunen, K. (1947). Über lineare Methoden in der Wahrscheinlichkeitsrechnung. *Suomalainen Tiedeakatemia*.
- [24] Loève, M. (1945). Fonctions aléatoires de second ordre. *Comptes Rendus Académie des Sciences*, 220, 469.
- [25] McKeown, M., Jung, T., Makeig, S., Brown, G., Kindermann, S., Lee, T., and Sejnowski, T. (1998a). Spatially independent activity patterns in functional MRI data during the stroop color-naming task. *Proc Natl Acad Sci USA* 95, 803-810.
- [26] McKeown, M., Makeig, S., Brown, G., Jung, T., Kindermann, S., Bell, A., and Sejnowski, T. (1998b). Analysis of fMRI data by blind separation into independent spatial components. *Hum Brain Mapp*, 6, 160-88.
- [27] McKeown, M. and Sejnowski, T. (1998c). Independent component analysis of fMRI data: examining the assumptions. *Hum. Brain Mapp*, 6, 368-372.
- [28] Meshulam, R., Moberg, P., Mahr, R., and Doty, R. (1998). Olfaction in neurodegenerative disease a meta-analysis of olfactory functioning in Alzheimer's and Parkinson's diseases. *Arch Neurol*, 55,84-90.
- [29] Prentice, R. and Pyke, R. (1979). Logistic disease incidence models and casecontrol studies. *Biometrika*, 66, 403-411.
- [30] Ramsay, J. and Silverman, B. (2006). Functional Data Analysis. *Springer-Verlag, New York*.

- [31] Schmithorst, V. and Holland, S. (2004). Comparison of three methods for generating group statistical inferences from independent component analysis of functional magnetic resonance imaging data. *J. Magn. Reson. Imaging*, 19 (3), 365-368.
- [32] Staniswalis, J. and Lee, J. (1998). Nonparametric regression analysis of longitudinal data. *Journal of the American Statistical Association*.
- [33] Tzourio-Mazoyer, N., Landeau, B., Papathanassiou, D., Crivello, F., Etard, O., Delcroix, N., Mazoyer, B., and Joliot, M. (2002). Automated anatomical labeling of activations in SPM using a macroscopic anatomical parcellation of the mni mri single-subject brain. *Neuroimage*, 15(1):273-289.
- [34] Yao, F., Müller, H., Clifford, A., Dueker, S., Follett, J., Lin, Y., Buchholz, B., and Vogel, J. (2003). Shrinkage estimation for functional principal component scores with application to the population. *Biometrics*.



	Eigenvalue	Eigenfunction
IC 1, PC 1	0.50	$\sqrt{2} \cos(\pi t)$
IC 1, PC 2	0.25	$\sqrt{2} \cos(2\pi t)$
IC 2, PC 1	0.50	$\sqrt{2} \sin(4\pi t)$
IC 2, PC 2	0.25	$\sqrt{2} \sin(6\pi t)$
IC 3, PC 1	0.50	$\sqrt{5}(6t^2 - 6t + 1)$
IC 3, PC 2	0.25	$\sqrt{7}(20t^3 - 30t^2 + 12t - 1)$

Table 1: Eigenvalues and Eigenfunctions of time courses used for simulation study

	Estimate	SE	LRT	Permutation Test
IC 11, PC 2	9.19	5.59	p = 0.028	p = 0.039
IC 13, PC 1	-5.44	3.40	p = 0.050	p = 0.071
IC 19, PC 3	-25.00	14.60	p = 0.016	p = 0.023
IC 22, PC 4	20.40	9.98	p = 0.009	p = 0.011
IC 26, PC 1	-3.70	2.13	p = 0.030	p = 0.039
IC 28, PC 1	7.82	4.90	p = 0.024	p = 0.043

Table 2: Univariate regression analysis results

	Estimate	SE	LRT	Permutation Test
IC 19 and 28, PC 2	-11.60	7.51	p = 0.007	p = 0.015
IC 22 and 28, PC 2	-36.80	28.40	p = 0.037	p = 0.050
IC 26 and 26, PC 3	-75.9	43.7	p = 0.026	p = 0.031

Table 3: Regression results using the functional connectivity as the predictors. IC 19 and 28 stands for the between network connectivity of spatial maps 19 and 28; IC 22 and 28 stands for the between network connectivity of spatial maps 22 and 28; IC 26 and 26 stands for the within network connectivity of spatial maps 26.

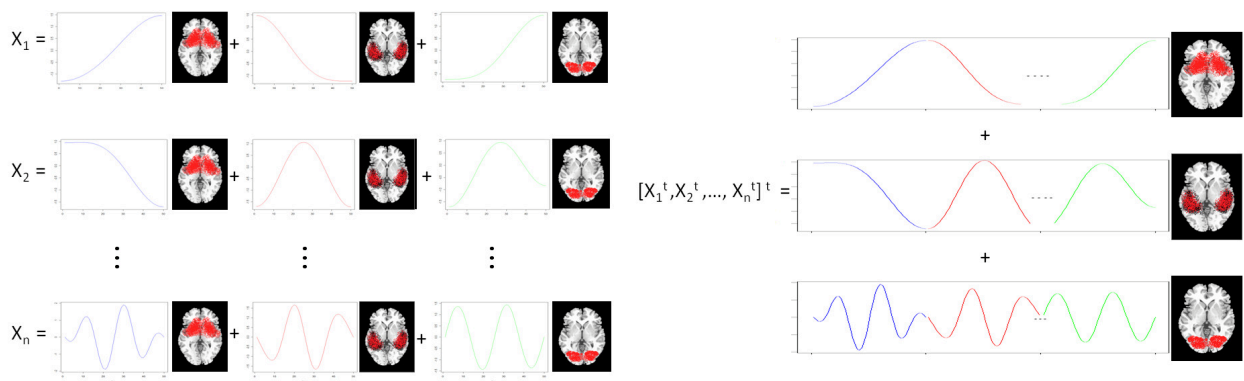


Figure 1: group ICA on temporally concatenated data

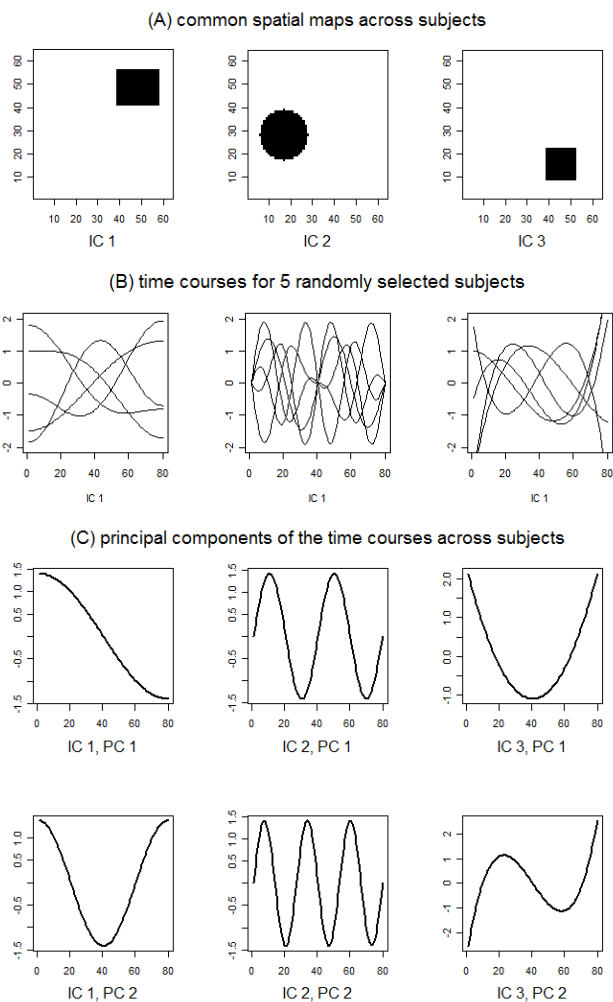


Figure 2: Spatial maps and time courses used for the simulation study. Panel (A) represents the spatial maps of the three independent components. Panel (B) displays the associated time courses of the three spatial maps for five randomly selected subjects. Panel (C) represents the principal components of the time courses. They are the main directions of variations of the time courses across subjects.

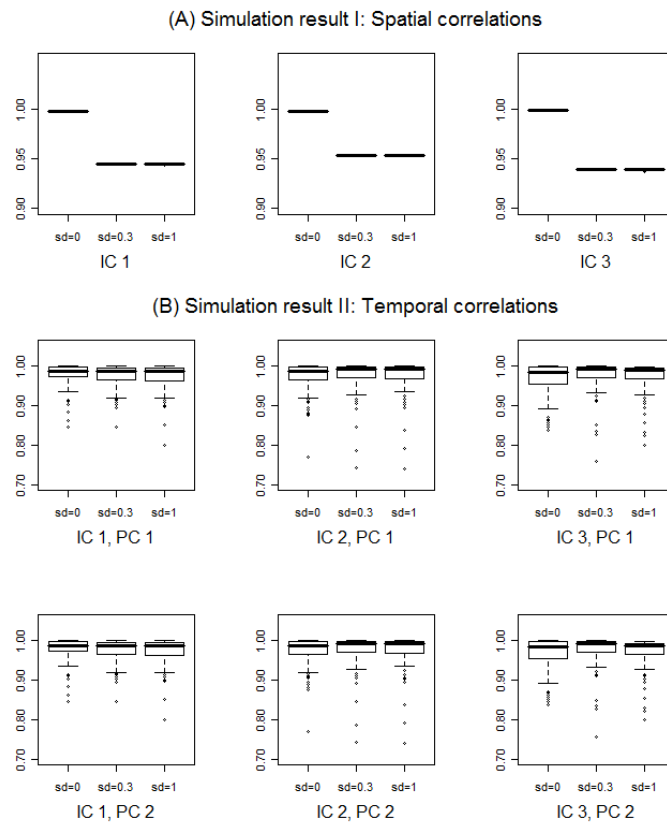


Figure 3: Box plots of correlations between the true and estimated spatial maps (A) and principal components of time courses (B). Three scenarios are considered in the simulation: the deviation for the Gaussian noise are 0, 0.3 and 1 respectively.

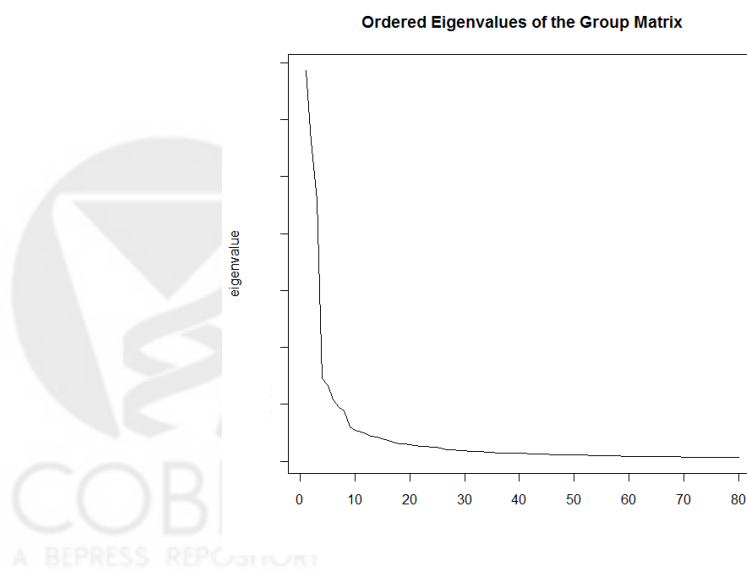


Figure 4: The first 80 ordered eigenvalues of the group data matrix.

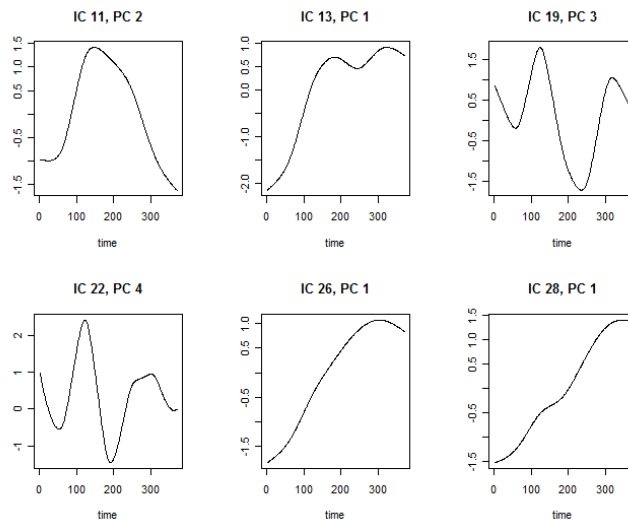


Figure 5: Plot of eigenfunctions associated with the significant predictors.

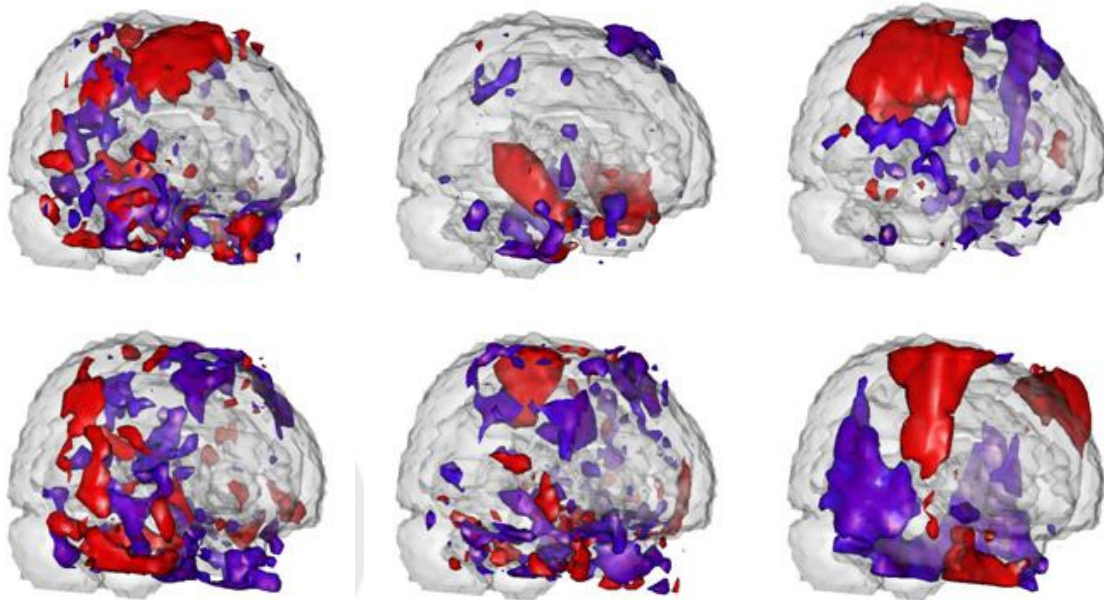


Figure 6: Three-D rendering of thresholded spatial maps associated with the significant predictors. Red areas load positively while blue areas load negatively. The figures from the upper left to the upper right are spatial maps of IC 11, 13 and 19 respectively. The figures from the lower left to the lower right are spatial maps of IC 22, 26 and 28 respectively.

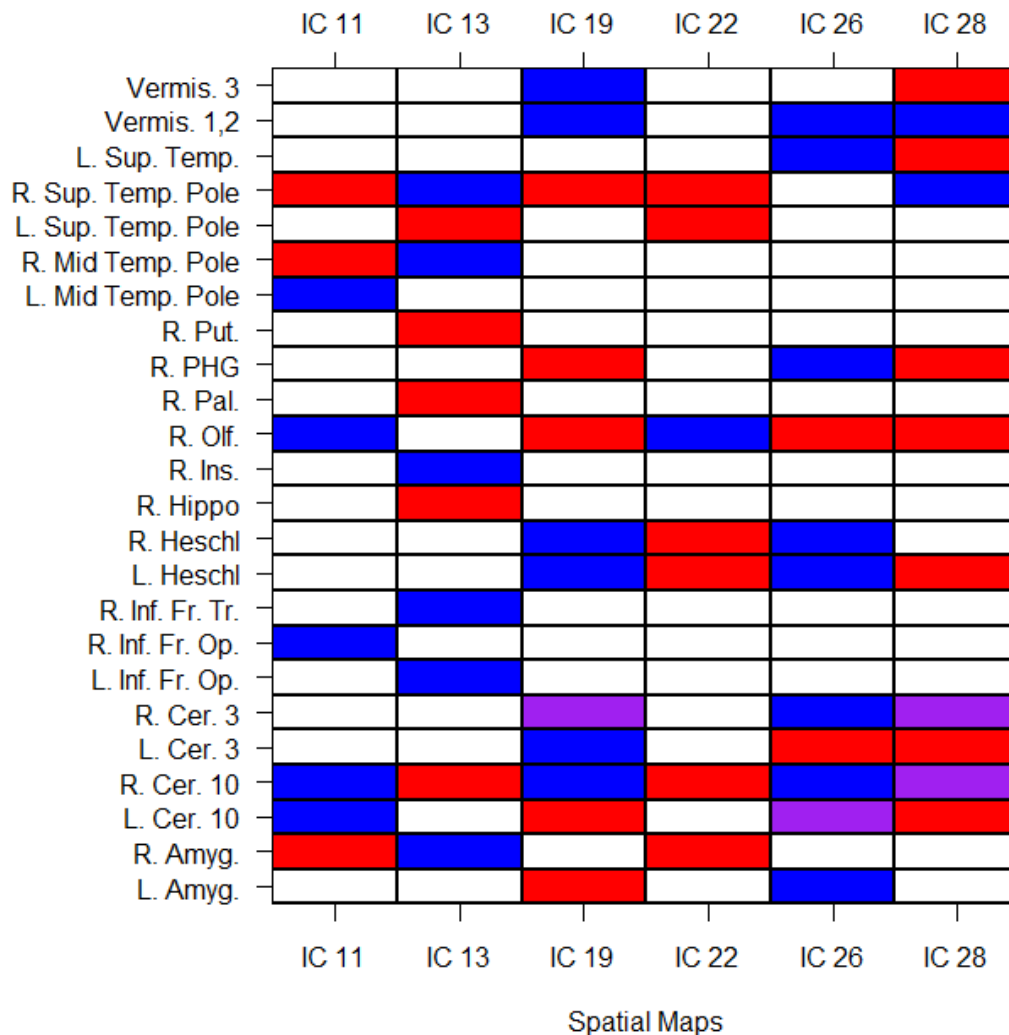


Figure 7: Regions with over 20% overlap with the specified spatial maps. Red areas load positively, blue negatively, purple have partial volumes loading positively and negatively. Abbreviations: Amyg. = Amygdala, Cer. = Cerebellum, Fr. = Frontal, Hippo = hippocampus, Inf. = Inferior, Ins. = Inusla, L. = Left, Olf. = Olfactory, Op. = Opercular part, Pal. = pallidum, PHG = Para-Hippocampal Gyrus, Put. = putamen, R. = Right, Sup. = Superior, Temp. = Temporal, Tri. = triangularis.